Pseudospin-lattice coupling and electric control of the square-lattice iridate Sr_2IrO_4

Feng Ye,[1] Christina Hoffmann,[1] Wei Tian,[1] Hengdi Zhao,[2] and G. Cao[2]
[1]*Neutron Scattering Division, Oak Ridge National Laboratory, Oak Ridge, Tennessee 37831, USA*
[2]*Department of Physics, University of Colorado at Boulder, Boulder, Colorado 80309, USA*

(Received 17 May 2020; revised 20 July 2020; accepted 26 August 2020; published 10 September 2020)

Sr_2IrO_4 is an archetypal spin-orbit-coupled Mott insulator and has been extensively studied in part because of a wide range of predicted states. Limited experimental characterization of these states thus far brings to light the extraordinary susceptibility of the physical properties to the lattice, particularly, the Ir-O-Ir bond angle. Here, we report a microscopic rotation of the IrO_6 octahedra below 50 K measured by single crystal neutron diffraction. This sharp lattice anomaly provides keys to understanding the anomalous low-temperature physics and a direct confirmation of a crucial role that the Ir-O-Ir bond angle plays in determining the ground state. Indeed, as also demonstrated in this study, applied electric current readily weakens the antiferromagnetic order via the straightening of the Ir-O-Ir bond angle, highlighting that even slight change in the local structure can disproportionately affect the physical properties in the spin-orbit-coupled system.

DOI: 10.1103/PhysRevB.102.115120

Strong spin-orbit interactions (SOI), along with appreciable Coulomb interactions, crystalline electric field, and large orbital hybridization in 5*d*-electron based oxides has produced a wide range of quantum phenomena such as spin liquid phases [1], superconductivity [2,3], and Kitaev magnetism [4–6]. One prominent example is the observation of the so-called effective $j_{\text{eff}} = 1/2$ Mott insulating state in iridates [7–9], where the magnetism is attributed to an isotropic pseudospin [10–12]. Unlike the situation in the 3*d* transition metal oxides which have a distinct energy scale in both orbital and spin parts and sequential orbital and magnetic orders, the notion of spin-orbital separation in the 5*d* systems is no longer valid due to the strong SOI. Furthermore, the Jahn-Teller effect, which measures the couples between the lattice and orbital degrees of freedom and is a common occurrence in 3*d*-electron based oxides, remains largely unexplored in the iridates. However, recent experimental and theoretical studies indicate that the magnetic properties and low-energy spin dynamics [13,14], can be better explained using a pseudospin-lattice coupling mechanism. The introduction of such a term in the spin Hamiltonian not only correctly describes the metamagnetic transitions [13], but also explains a finite in-plane magnon gap [15–17]. It also predicts an orthorhombic structural distortion in the order of 10^{-4}, which can be probed using a high resolution Larmor precession technique [18].

The extraordinarily strong coupling between the electronic and structural properties in the iridates provides unprecedented opportunities to uncover quantum phases by merely modifying the local structure. It is particularly interesting that application of hydrostatic pressure steadily reduces the charge gap of approximately 500 meV and diminishes the antiferromagnetic (AFM) state existent in the square lattice Sr_2IrO_4 (Sr-214), yet retains the insulating state [19–21]. A possible quantum paramagnetic state at pressures greater than 20 GPa is proposed, attributing to the suppression of the interlayer exchange coupling and enhanced magnetic frustration within the IrO_2 layer [22]. Alternative approaches to modify the structure using strain engineering are also reported in epitaxial grown thin films of Sr-214 [23–27], where a compressive or tensile strain can drastically enhance or reduce the transition temperature T_N. In some cases, the strengthened in-plane exchange interaction can promote a short-range magnetic correlation well above the nominal transition [27]. In this paper, we report a lattice anomaly observed at 50 K Given the exceptionally strong coupling between the lattice and physical properties in Sr-214, this structural anomaly has escaped all previous studies until now. Our study provides much-needed keys to better understand the low-temperature magnetic and transport behavior, which remains a focus of current studies on the iridates. Indeed, the susceptibility of the physical properties to the lattice is further revealed by the application of in-plane *dc* electric current as a stimulus that straightens the Ir-O-Ir bond angle, thus suppressing the canted AFM order. These results reveal crucial insights into the crystal structure and demonstrates that the subtle changes in the crystal structure, whether ambient or induced, dictate the physical properties in this spin-orbit-coupled Mott insulator.

Single crystals of Sr-214 were grown using the self-flux method [28,29]. The magnetic susceptibility and specific heat were measured using a Quantum Design Magnetic Property Measurement System. The neutron diffraction measurements were carried out at the HB1A triple axis spectrometer at the High Flux Isotope Reactor and the TOPAZ diffractometer at the Spallation Neutron Source, ORNL. For measurements at HB1A, a sample assembly of over 40 single crystals (mass ~25 mg, mosaicity ~1.5°) was aligned at various scattering planes to probe the magnetic and nuclear reflections. A closed-cycle refrigerator was used to regulate the sample temperature (T). For measurements at TOPAZ, a platelike single crystal with dimensions of 1.8 mm × 1.8 mm × 0.55 mm was used. The sample temperature is controlled using the Oxford cryostream cooler Cobra 800. Electric current was applied

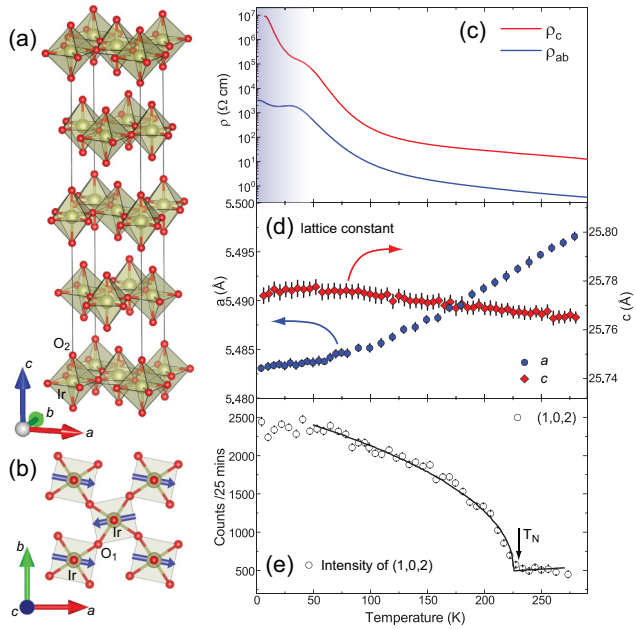

FIG. 1. (a) The crystal structure of Sr_2IrO_4 in the tetragonal setting. For simplicity, only the iridium and oxygen atoms are shown. (b) The connecting IrO_6 network is viewed along the c axis. The T dependence of (c) the in-plane and c-axis resistivity $\rho_{ab}(T)$ and $\rho_c(T)$, (d) the lattice parameters a and c measured from neutron diffraction, and (e) the strongest AFM peak (1,0,2). The solid line in panel (e) is a guide to the eye.

using the power supply from BioLogic science potentiostat with a voltage range of ± 12 V and current range ± 200 mA.

Figures 1(a) and 1(b) show the main structural features of the Sr-214 with Ir ions forming a square-lattice network. The system exhibits a characteristic staggered rotation of IrO_6 octahedra along the c axis at about $\approx 11.8^\circ$ [30,31]. Because of the layered structure, the corresponding IrO_6 octahedra elongate slightly along the c axis causing a crystal electric field (CEF) level $\Delta_{CEF} \sim 200$ meV [4,32]. Neutron scattering studies reveal a long-range magnetic order below 240 K [Fig. 1(e)]. Magnetic structure refinement indicates that the spins of Ir ions form a canted AFM configuration. The in-plane magnetic components closely track the rotation of the IrO_6 [31,33], which results directly from the SOI; the canting angle is governed by a characteristic ratio, $\phi \sim D/2J$, of the antisymmetric Dzyaloshinskii-Moriya (DM) interaction D to the isotropic Heisenberg interaction J [4].

It is known that the onset of long-range magnetic order at T_N causes no anomaly in ρ_{ab} or ρ_c [28,34], specific heat (data not shown), and the lattice parameters [Figs. 1(c)–1(d)]. The conventionally anticipated correlation between the structural and physical properties is conspicuously missing at T_N. However, such a correlation is instead established below an observed lattice anomaly, $T_M = 50$ K. As shown in Fig. 1(c), both the in-plane and c-axis resistivity exhibit noticeable kinks below T_M. Recently, independent experiments have confirmed the anomalous character at low T. Among them, a magnetic study shows that the residual magnetization increases below T_N, peaks at T_M, and diminishes on further cooling [35]. Such behavior was initially attributed to the reorientation of the canted spin moment [34]. A muon spin rotation study by Franke *et al.* shows that the oscillation of the single precession signal below the magnetic transition splits into high and low frequency components below 20 K [36]. The authors of Ref. [36] suggest that the modification of the magnetic structure leads to structurally equivalent muon sites that experience increasingly distinct local field at low temperatures.

Nevertheless, the abnormal low-T behavior demands a detailed examination of the crystal structure. The neutron diffraction measurements indicate that the system remains tetragonal at all temperature and does not show a lower symmetry below the magnetic transition [30,31,37,38]. Since the neutron coherent scattering length of the light oxygen atom ($b_O = 5.8$ fm) is comparable to the much heavier strontium ($b_{Sr} = 7.02$ fm) and iridium ($b_{Ir} = 10.6$ fm), the subtle change of the IrO_6 rotation can be readily characterized using neutron diffraction and used to quantify its coupling to the magnetic order. The structure factor of the nuclear scattering at a wave-vector transfer $\vec{q}$ is

$$|F(\vec{q})|^2 = \left| \sum_i b_i \exp(\vec{r}_i \cdot \vec{q}) \right|^2, \quad (1)$$

where b_i is the coherent scattering length for individual atom inside the unit cell and $\vec{r}_i$ is the corresponding atomic coordinate. The rotation of the IrO_6 octahedra leads to the nonzero peak intensities forbidden for the space group $I4/mmm$, e.g., $(2, 1, 2n + 1)$, and is solely determined by the in-plane oxygen atom O_1 located at $(1/4 - \delta, 1/2 - \delta, 1/8)$ and equivalent positions, where $\delta \approx 0.05$ characterizes the deviation from the undistorted IrO_6 scenario. The intensity of the superlattice peak (2,1,1), I_{211}, can be derived as $b_O(\sin\delta + \sin 3\delta)^2$ and is proportional to δ^2 in the small rotation limit.

The red squares in Fig. 2(c) show the (2, 1, 1) peak intensity upon cooling. The gradual increase in intensity implies an enhancement of the IrO_6 rotation. Surprisingly, the monotonic evolution experiences an abrupt change below 50 K. To further verify the feature, $\theta - 2\theta$ scans across the peak are performed (blue circles). The marked decrease at low-T reveals that the suppression of IrO_6 octahedral rotation is intrinsic. Comparing to 50 K, the value at 5 K is reduced by 5%, which translates to a suppression of rotation angle by 0.3°. As the moment strictly follows the octahedral rotation, one expects a sudden reduction of the rotation or straightening of the Ir-O-Ir bond angle. This can be probed by examining the magnetic reflection (0, 0, 3) that is exclusively sensitive to the canted component [31]. Figure 2(b) displays the T dependence of the magnetic peak with long counting time. A similar kink is observed below 50 K, reinforcing the structural anomaly in Fig. 2(c). This is also consistent with the abrupt reduction of the magnetization shown in Fig. 2(a) with an external magnetic field of $\mu_0 H = 0.1$ T applied along either the [1, 0, 0] or the [1, 1, 0] directions, which also agrees well with our earlier report [39]. These data point out a close association between the crystal structure and magnetic order, confirming an essential role of the pseudospin-lattice coupling that dictates the low-energy magnetic properties.

This key characteristic of the lattice degree of freedom provides an effective "knob" to control the physical properties

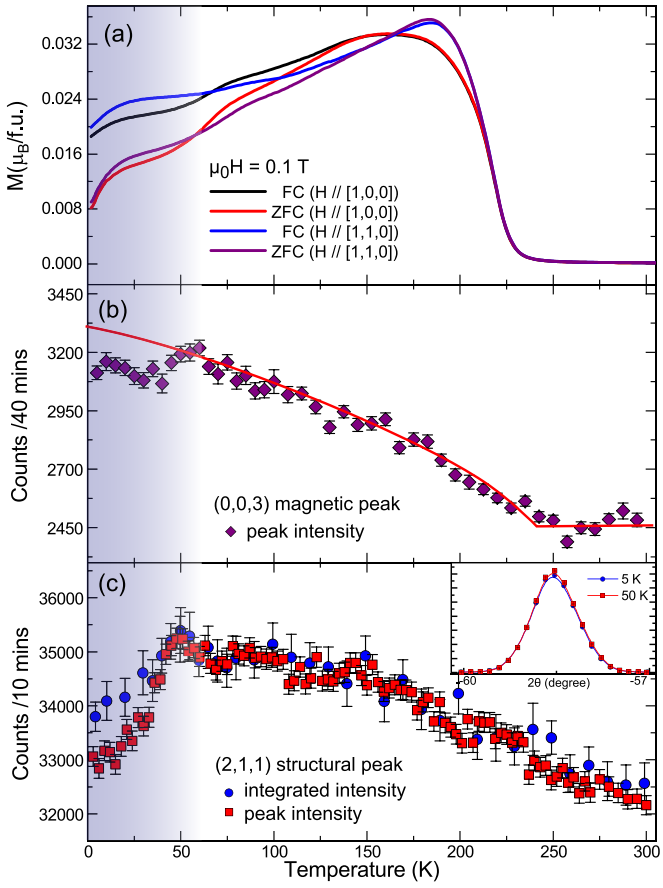

FIG. 2. (a) The magnetization M in the zero-field-cooled (ZFC) and field-cooled (FC) protocols, with a magnetic field of 0.1 Tesla applied along the [1, 0, 0] and [1, 1, 0] directions. (b) The T dependence of the peak intensity of the magnetic (0,0,3) reflection which probes the canted spin component. The solid line is a guide to the eye. (c) The T evolution of the structural peak (2,1,1) associated with the in-plane rotation of the IrO_6 octahedra. The (blue) circles are the integrated intensities, the (red) squares are the peak intensities. Inset shows the comparison of the $\theta - 2\theta$ scans at 5 and 50 K. Both peaks are fit using Gaussian profile.

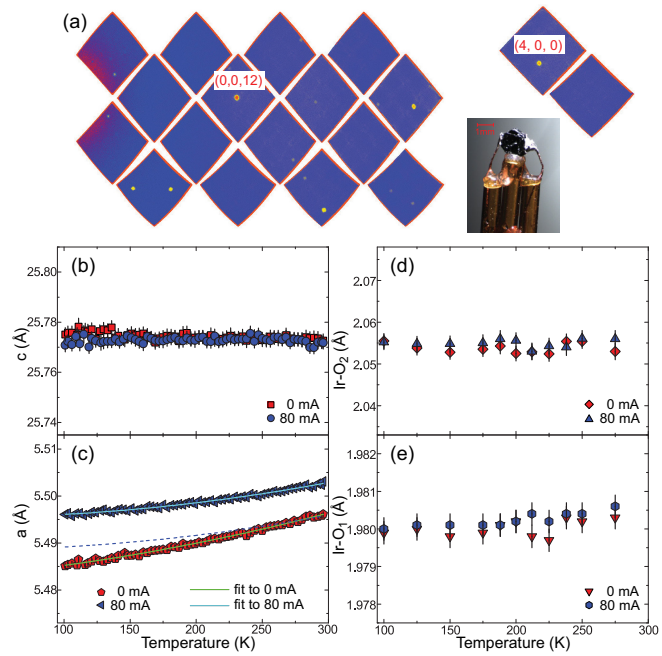

FIG. 3. (a) The TOPAZ instrument view of the diffraction experiment. The sample is oriented to allow optimal collection of desired reflections based on the physical layout of detector modules. The inset shows the experimental setup for applying electric current. The temperature is regulated using active cryostream cooling to ensure the sample is in thermal equilibrium [40]. The T dependence of the lattice parameters c [panel (b)] and a [panel (c)] without and with applied electric current of 80 mA. The solid green and light blue curves are quadratic fits of the lattice parameters. The light blue curve is also shifted down vertically by 0.007 Å (the dashed blue curve) to match the $I = 0$ mA data above the magnetic transition. The corresponding refined out-of-plane Ir-O_2 and in-plane Ir-O_1 bond distance are shown in panels (d) and (e).

of the iridates using small external stimuli that readily couple to the lattice. Electrical current, as a stimulus, is particularly effective in controlling the lattice, and thus the magnetic properties [41]. The previous x-ray study has shown a prominent lattice expansion for the undoped Sr-214 under electric current, accompanied by remarkable reduction in both transition temperature and in-plane magnetization. No structural anomaly is observed in Tb-doped Sr-214 where long-range magnetic order is absent [42]. To better characterize the structural response, we perform single crystal neutron diffraction measurements with *in situ* electric current application. The orientation of the Sr-214 crystal is determined using the x-ray Laue method to ensure the currents are applied in the basal plane [inset of Fig. 3]. Since the diffractometer TOPAZ has a white incident neutron beam with large reciprocal coverage, the sample is mounted such that the characteristic (4, 0, 0) and (0, 0, 12) peaks can be simultaneously accessed [Fig. 3(a)]. In such a fixed-orientation configuration, we collected a total number of around 2000 nuclear reflections at each temperature that allow a reliable structural determination. A electric current of 80 mA (current density ~8 A/cm^2) is employed at 300 K and the sample is cooled to 100 K, while the electric current is maintained. The crystal is subsequently warmed to 300 K at a rate of 0.5 K/min. Figures 3(b) and 3(c) display the T dependence for the out-of-plane and in-plane lattice parameters with and without electric current, respectively. It is evident that the c-axis lattice parameter is insensitive to the current. In contrast, the in-plane lattice parameter displays a dramatic response to the current, consistent with the fact that the magnetic moments lie within the basal plane. The overall T dependence of lattice parameter a at 80 mA stays above the one at $I = 0$. While both data can be well described by a quadratic form, a slope change near the AFM transition is clearly visible [see the dashed curve in Fig. 3(c)]. The detailed structure refinement reveals that the Ir-O bond distances remain unchanged at $I = 80$ mA. The corresponding IrO_6 octahedron also remains slightly elongated, with a ratio of the Ir-O_2 to the Ir-O_1 bond distances being 1.04 throughout the temperature range measured.

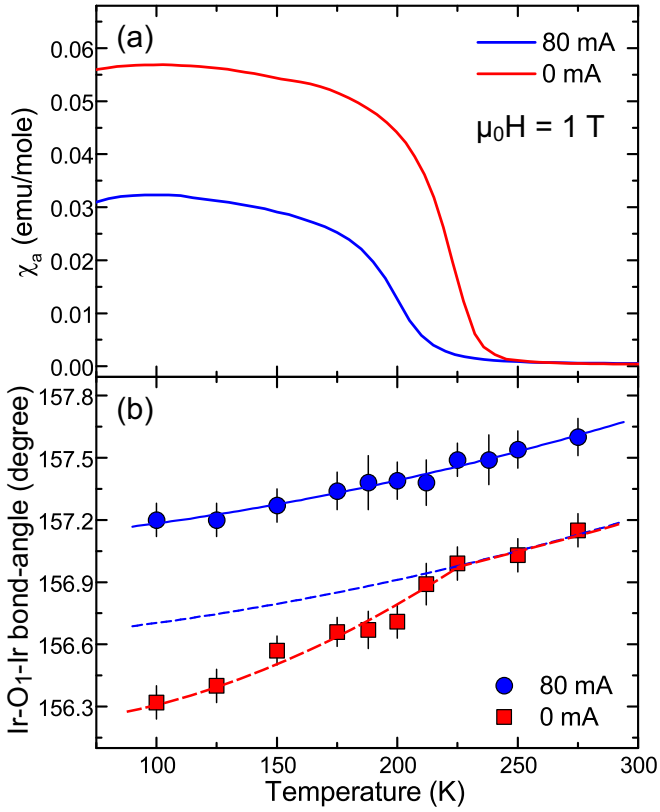

FIG. 4. The magnetic susceptibility $\chi(T)$ with electric current of I=0 and 80 mA applied in the basal plane. (b) The T dependence of refined in-plane Ir-O_1-Ir bond angle with and without electric current.

Although the IrO_6 octahedra remain rigid irrespective of the applied electric current, the in-plane Ir-O-Ir bond angle between the corner-sharing IrO_6 octahedra undergoes a considerable modification. Figure 4(b) compares the refined bond angle between the two situations. The angle at 0 mA stays smaller than 157° and decreases with further reduction of temperature. A slope change occurs at the magnetic transition T_N at $I = 0$ mA. In sharp contrast, the bond angle becomes notably straighter or relaxed by 0.3° when a current of $I = 80$ mA is applied in the basal plane. In addition, these bond angle values show a smooth decrease upon cooling; the anomaly observed near T_N at the ambient condition is significantly suppressed. Indeed, the corresponding in-plane magnetic susceptibility displays the behavior consistent with the structural data [Fig. 4(b)]. The χ_a at 80 mA shows reduction in amplitude along with the suppression and broadening of the transition temperature. The reduced magnetization is expected because the DM interaction D becomes smaller as the Ir-O-Ir bond angle relaxes due to the applied current (recall $\phi \sim D/2J$).

Tuning the physical properties, in particular magnetism using electric current, is highly desirable. It opens a different frontier for studies of the correlated and spin-orbit-coupled systems [41,43,44]. For instance, a reorientation of the AFM order is observed in the metallic $Fe_{1/3}NbS_2$ at a remarkable low current density ($\sim 10^4$ A/cm^2) showing the potential to build AFM spintronics devices [43]. Spatially inhomogeneous rotation of the skyrmion lattice in the metallic helimagnet MnSi occurs when a current flows across the sample. This emphasizes the role of friction near the sample edges for skyrmion-based applications [44]. Much effort has also been devoted to *insulating* materials such as ruthenate oxide Ca_2RuO_4 [40,45–50]. Zhao *et al.* have shown that a extremely small electric current density ($\sim$0.15 A/cm^2) can reduce the orthorhombic distortion and AFM order, and further induce an orbital state featuring a simultaneous jump in both magnetization and electrical resistivity [40]. The authors propose that orbital occupancies stabilized by the nonequilibrium current drive the lattice changes and the related phenomena. Because of the distinct energy hierarchy in the SOI system, the narrow band Mott insulator Sr-214 is more susceptible to such a perturbative approach. It is anticipated the crystallographic details through this structural study would feed critical information for the electronic band structure calculations, and assist to explain the emerging phenomena including the negative differential resistivity, reversible resistance switching in Sr-214 [41,51,52], and the nonlinear conductivity in other spin-orbit-coupled iridates [53,54].

In summary, neutron diffraction work of the square lattice Sr-214 reveals a pronounced reduction of the staggered IrO_6 distortion below 50 K. This important observation will help us better understand the low-temperature physics of the archetypal spin-orbit-couple Mott insulator as the magnetic and transport properties closely tracks the underlying lattice. This point is further strengthened in that applying a steady electric current at 8A/cm^2 readily reduces the in-plane IrO_6 octahedral rotation, which aligns well with the diminishing bulk magnetization. Our study demonstrates that the application of electric current is an effective and appealing route to tune the lattice and probe the rich physics in the SOI system.

We thank Dr. G. Jackeli for stimulating discussion. We acknowledge Dr. B. Hu for her help in the magnetization measurement and the technical support for the electric current measurement from J. He, G. Rucker. and H. Skorpenske. This research used resources at the Spallation Neutron Source and the High Flux Isotope Reactor, which are DOE Office of Science User Facilities operated by the Oak Ridge National Laboratory. Work at the University of Colorado was supported by the U.S. National Science Foundation via Grant No. DMR-1903888.

[1] Y. Okamoto, M. Nohara, H. Aruga-Katori, and H. Takagi, Spin-Liquid State in the S = 1/2 Hyperkagome Antiferromagnet $Na_4Ir_3O_8$, Phys. Rev. Lett. **99**, 137207 (2007).

[2] F. Wang and T. Senthil, Twisted Hubbard Model for Sr_2IrO_4: Magnetism and Possible High Temperature Superconductivity, Phys. Rev. Lett. **106**, 136402 (2011).

[3] H. Watanabe, T. Shirakawa, and S. Yunoki, Monte Carlo Study of an Unconventional Superconducting Phase in Iridium Oxide $J_{\mathrm{eff}} = 1/2$ Mott Insulators Induced by Carrier Doping, Phys. Rev. Lett. **110**, 027002 (2013).

[4] G. Jackeli and G. Khaliullin, Mott Insulators in the Strong Spin-Orbit Coupling Limit: From Heisenberg to a Quantum Compass and Kitaev Models, Phys. Rev. Lett. **102**, 017205 (2009).

[5] C. C. Price and N. B. Perkins, Critical Properties of the Kitaev-Heisenberg Model, Phys. Rev. Lett. **109**, 187201 (2012).

[6] Y. Singh, S. Manni, J. Reuther, T. Berlijn, R. Thomale, W. Ku, S. Trebst, and P. Gegenwart, Relevance of the Heisenberg-Kitaev Model for the Honeycomb Lattice Iridates A_2IrO_3, Phys. Rev. Lett. **108**, 127203 (2012).

[7] B. J. Kim, H. Jin, S. J. Moon, J.-Y. Kim, B.-G. Park, C. S. Leem, J. Yu, T. W. Noh, C. Kim, S.-J. Oh, J.-H. Park, V. Durairaj, G. Cao, and E. Rotenberg, Novel $J_{\mathrm{eff}} = 1/2$ Mott State Induced by Relativistic Spin-Orbit Coupling in Sr_2IrO_4, Phys. Rev. Lett. **101**, 076402 (2008).

[8] S. J. Moon, H. Jin, K. W. Kim, W. S. Choi, Y. S. Lee, J. Yu, G. Cao, A. Sumi, H. Funakubo, C. Bernhard, and T. W. Noh, Dimensionality-Controlled Insulator-Metal Transition and Correlated Metallic State in 5*d* Transition Metal Oxides $Sr_{n+1}Ir_nO_{3n+1}$ ($n = 1$, 2, and ∞), Phys. Rev. Lett. **101**, 226402 (2008).

[9] B. J. Kim, H. Ohsumi, T. Komesu, S. Sakai, T. Morita, H. Takagi, and T. Arima, Phase-sensitive observation of a spin-orbital Mott state in Sr_2IrO_4, Science **323**, 1329 (2009).

[10] J. G. Rau, E. K.-H. Lee, and H.-Y. Kee, Spin-orbit physics giving rise to novel phases in correlated systems: Iridates and related materials, Annu. Rev. Condens. Matter Phys. **7**, 195 (2016).

[11] S. M. Winter, A. A. Tsirlin, M. Daghofer, J. van den Brink, Y. Singh, P. Gegenwart, and R. Valentí, Models and materials for generalized Kitaev magnetism, J. Phys.: Condens. Matter **29**, 493002 (2017).

[12] M. Hermanns, I. Kimchi, and J. Knolle, Physics of the Kitaev model: Fractionalization, dynamic correlations, and material connections, Annu. Rev. Condens. Matter Phys. **9**, 17 (2018).

[13] J. Porras, J. Bertinshaw, H. Liu, G. Khaliullin, N. H. Sung, J.-W. Kim, S. Francoual, P. Steffens, G. Deng, M. M. Sala, A. Efimenko, A. Said, D. Casa, X. Huang, T. Gog, J. Kim, B. Keimer, and B. J. Kim, Pseudospin-lattice coupling in the spin-orbit Mott insulator Sr_2IrO_4, Phys. Rev. B **99**, 085125 (2019).

[14] H. Liu and G. Khaliullin, Pseudo-Jahn-Teller Effect and Magnetoelastic Coupling in Spin-Orbit Mott Insulators, Phys. Rev. Lett. **122**, 057203 (2019).

[15] Y. Gim, A. Sethi, Q. Zhao, J. F. Mitchell, G. Cao, and S. L. Cooper, Isotropic and anisotropic regimes of the field-dependent spin dynamics in Sr_2IrO_4: Raman scattering studies, Phys. Rev. B **93**, 024405 (2016).

[16] H. Gretarsson, J. Sauceda, N. H. Sung, M. Höppner, M. Minola, B. J. Kim, B. Keimer, and M. Le Tacon, Raman scattering study of vibrational and magnetic excitations in $Sr_{2-x}La_xIrO_4$, Phys. Rev. B **96**, 115138 (2017).

[17] S. Calder, D. M. Pajerowski, M. B. Stone, and A. F. May, Spin-gap and two-dimensional magnetic excitations in Sr_2IrO_4, Phys. Rev. B **98**, 220402 (2018).

[18] F. Li, H. Feng, A. N. Thaler, S. R. Parnell, W. A. Hamilton, L. Crow, W. Yang, A. B. Jones, H. Bai, M. Matsuda, D. V. Baxter, T. Keller, J. A. Fernandez-Baca, and R. Pynn, High resolution neutron Larmor diffraction using superconducting magnetic Wollaston prisms, Sci. Rep. **7**, 865 (2017).

[19] D. A. Zocco, J. J. Hamlin, B. D. White, B. J. Kim, J. R. Jeffries, S. T. Weir, Y. K. Vohra, J. W. Allen, and M. B. Maple, Persistent non-metallic behavior in Sr_2IrO_4 and $Sr_3Ir_2O_7$ at high pressures, J. Phys.: Condens. Matter **26**, 255603 (2014).

[20] C. Chen, Y. Zhou, X. Chen, T. Han, C. An, Y. Zhou, Y. Yuan, B. Zhang, S. Wang, R. Zhang, L. Zhang, C. Zhang, Z. Yang, L. E. DeLong, and G. Cao, Persistent insulating state at megabar pressures in strongly spin-orbit coupled Sr_2IrO_4, Phys. Rev. B **101**, 144102 (2020).

[21] K. Samanta, R. Tartaglia, U. F. Kaneko, N. M. Souza-Neto, and E. Granado, Anisotropic lattice compression and pressure-induced electronic phase transitions in Sr_2IrO_4, Phys. Rev. B **101**, 075121 (2020).

[22] D. Haskel, G. Fabbris, J. H. Kim, L. S. I. Veiga, J. R. L. Mardegan, C. A. Escanhoela, S. Chikara, V. Struzhkin, T. Senthil, B. J. Kim, G. Cao, and J.-W. Kim, Possible Quantum Paramagnetism in Compressed Sr_2IrO_4, Phys. Rev. Lett. **124**, 067201 (2020).

[23] A. Lupascu, J. P. Clancy, H. Gretarsson, Z. Nie, J. Nichols, J. Terzic, G. Cao, S. S. A. Seo, Z. Islam, M. H. Upton, J. Kim, D. Casa, T. Gog, A. H. Said, V. M. Katukuri, H. Stoll, L. Hozoi, J. van den Brink, and Y.-J. Kim, Tuning Magnetic Coupling in Sr_2IrO_4 Thin Films with Epitaxial Strain, Phys. Rev. Lett. **112**, 147201 (2014).

[24] L. Miao, H. Xu, and Z. Q. Mao, Epitaxial strain effect on the $J_{\mathrm{eff}} = 1/2$ moment orientation in Sr_2IrO_4 thin films, Phys. Rev. B **89**, 035109 (2014).

[25] C. Lu, S. Dong, A. Quindeau, D. Preziosi, N. Hu, and M. Alexe, Dual gate control of bulk transport and magnetism in the spin-orbit insulator Sr_2IrO_4, Phys. Rev. B **91**, 104401 (2015).

[26] B. Kim, B. H. Kim, K. Kim, and B. I. Min, Substrate-tuning of correlated spin-orbit oxides revealed by optical conductivity calculations, Sci. Rep. **6**, 27095 (2016).

[27] A. Seo, P. P. Stavropoulos, H.-H. Kim, K. Fürsich, M. Souri, J. G. Connell, H. Gretarsson, M. Minola, H. Y. Kee, and B. Keimer, Compressive strain induced enhancement of exchange interaction and short-range magnetic order in Sr_2IrO_4 investigated by Raman spectroscopy, Phys. Rev. B **100**, 165106 (2019).

[28] G. Cao, J. Bolivar, S. McCall, J. E. Crow, and R. P. Guertin, Weak ferromagnetism, metal-to-nonmetal transition, and negative differential resistivity in single-crystal Sr_2IrO_4, Phys. Rev. B **57**, R11039 (1998).

[29] G. Cao and P. Schlottmann, The challenge of spin–orbit-tuned ground states in iridates: A key issues review, Rep. Prog. Phys. **81**, 042502 (2018).

[30] Q. Huang, J. L. Soubeyroux, O. Chmaissem, I. N. Sora, A. Santoro, R. J. Cava, J. J. Krajewski, and W. F. Peck, Neutron Powder diffraction study of the crystal-structures of Sr_2RuO_4 and Sr_2IrO_4 at room-temperature and at 10-K, J. Solid State Chem. **112**, 355 (1994).

[31] F. Ye, S. Chi, B. C. Chakoumakos, J. A. Fernandez-Baca, T. Qi, and G. Cao, Magnetic and crystal structures of Sr_2IrO_4: A neutron diffraction study, Phys. Rev. B **87**, 140406(R) (2013).

[32] S. J. Moon, M. W. Kim, K. W. Kim, Y. S. Lee, J.-Y. Kim, J.-H. Park, B. J. Kim, S.-J. Oh, S. Nakatsuji, Y. Maeno, I. Nagai, S. I. Ikeda, G. Cao, and T. W. Noh, Electronic structures of

layered perovskite Sr_2MO_4(M = Ru, Rh, and Ir), Phys. Rev. B **74**, 113104 (2006).

[33] S. Boseggia, H. C. Walker, J. Vale, R. Springell, Z. Feng, R. S. Perry, M. M. Sala, H. M. Rønnow, S. P. Collins, and D. F. McMorrow, Locking of iridium magnetic moments to the correlated rotation of oxygen octahedra in Sr_2IrO_4 revealed by x-ray resonant scattering, J. Phys.: Condens. Matter **25**, 422202 (2013).

[34] S. Chikara, O. Korneta, W. P. Crummett, L. E. DeLong, P. Schlottmann, and G. Cao, Giant magnetoelectric effect in the $J_{\rm eff} = 1/2$ Mott insulator Sr_2IrO_4, Phys. Rev. B **80**, 140407 (2009).

[35] I. N. Bhatti and A. K. Pramanik, Insight into the magnetic behavior of Sr_2IrO_4: A spontaneous magnetization study, Phys. Lett. A **383**, 1806 (2019).

[36] I. Franke, P. J. Baker, S. J. Blundell, T. Lancaster, W. Hayes, F. L. Pratt, and G. Cao, Measurement of the internal magnetic field in the correlated iridates Ca_4IrO_6, $Ca_5Ir_3O_{12}$, $Sr_3Ir_2O_7$ and Sr_2IrO_4, Phys. Rev. B **83**, 094416 (2011).

[37] C. Dhital, T. Hogan, Z. Yamani, C. de la Cruz, X. Chen, S. Khadka, Z. Ren, and S. D. Wilson, Neutron scattering study of correlated phase behavior in Sr_2IrO_4, Phys. Rev. B **87**, 144405 (2013).

[38] F. Ye, X. Wang, C. Hoffmann, J. Wang, S. Chi, M. Matsuda, B. C. Chakoumakos, J. A. Fernandez-Baca, and G. Cao, Structure symmetry determination and magnetic evolution in $Sr_2Ir_{1-x}Rh_xO_4$, Phys. Rev. B **92**, 201112 (2015).

[39] M. Ge, T. F. Qi, O. B. Korneta, D. E. De Long, P. Schlottmann, W. P. Crummett, and G. Cao, Lattice-driven magnetoresistivity and metal-insulator transition in single-layered iridates, Phys. Rev. B **84**, 100402 (2011).

[40] H. Zhao, B. Hu, F. Ye, C. Hoffmann, I. Kimchi, and G. Cao, Nonequilibrium orbital transitions via applied electrical current in calcium ruthenates, Phys. Rev. B **100**, 241104 (2019).

[41] G. Cao, J. Terzic, H. D. Zhao, H. Zheng, L. E. De Long, and P. S. Riseborough, Electrical Control of Structural and Physical Properties via Strong Spin-Orbit Interactions in Sr_2IrO_4, Phys. Rev. Lett. **120**, 017201 (2018).

[42] J. C. Wang, S. Aswartham, F. Ye, J. Terzic, H. Zheng, D. Haskel, S. Chikara, Y. Choi, P. Schlottmann, R. Custelcean, S. J. Yuan, and G. Cao, Decoupling of the antiferromagnetic and insulating states in Tb-doped Sr_2IrO_4, Phys. Rev. B **92**, 214411 (2015).

[43] N. L. Nair, E. Maniv, C. John, S. Doyle, J. Orenstein, and J. G. Analytis, Electrical switching in a magnetically intercalated transition metal dichalcogenide, Nat. Mater. **19**, 153 (2019).

[44] D. Okuyama, M. Bleuel, J. S. White, Q. Ye, J. Krzywon, G. Nagy, Z. Q. Im, I. Živković, M. Bartkowiak, H. M. Rønnow, S. Hoshino, J. Iwasaki, N. Nagaosa, A. Kikkawa, Y. Taguchi, Y. Tokura, D. Higashi, J. D. Reim, Y. Nambu, and T. J. Sato, Deformation of the moving magnetic skyrmion lattice in MnSi under electric current flow, Commun. Phys. **2**, 79 (2019).

[45] F. Nakamura, M. Sakaki, Y. Yamanaka, S. Tamaru, T. Suzuki, and Y. Maeno, Electric-field-induced metal maintained by current of the Mott insulator Ca_2RuO_4, Sci. Rep. **3**, 2536 (2013).

[46] R. Okazaki, Y. Nishina, Y. Yasui, F. Nakamura, T. Suzuki, and I. Terasaki, Current-induced gap suppression in the Mott insulator Ca_2RuO_4, J. Phys. Soc. Jpn. **82**, 103702 (2013).

[47] J. Bertinshaw, N. Gurung, P. Jorba, H. Liu, M. Schmid, D. T. Mantadakis, M. Daghofer, M. Krautloher, A. Jain, G. H. Ryu, O. Fabelo, P. Hansmann, G. Khaliullin, C. Pfleiderer, B. Keimer, and B. J. Kim, Unique Crystal Structure of Ca_2RuO_4 in the Current Stabilized Semimetallic State, Phys. Rev. Lett. **123**, 137204 (2019).

[48] J. Zhang, A. S. McLeod, Q. Han, X. Chen, H. A. Bechtel, Z. Yao, S. N. Gilbert Corder, T. Ciavatti, T. H. Tao, M. Aronson, G. L. Carr, M. C. Martin, C. Sow, S. Yonezawa, F. Nakamura, I. Terasaki, D. N. Basov, A. J. Millis, Y. Maeno, and M. Liu, Nano-Resolved Current-Induced Insulator-Metal Transition in the Mott Insulator Ca_2RuO_4, Phys. Rev. X **9**, 011032 (2019).

[49] C. Cirillo, V. Granata, G. Avallone, R. Fittipaldi, C. Attanasio, A. Avella, and A. Vecchione, Emergence of a metallic metastable phase induced by electrical current in Ca_2RuO_4, Phys. Rev. B **100**, 235142 (2019).

[50] K. Fürsich, J. Bertinshaw, P. Butler, M. Krautloher, M. Minola, and B. Keimer, Raman scattering from current-stabilized nonequilibrium phases in Ca_2RuO_4, Phys. Rev. B **100**, 081101 (2019).

[51] O. B. Korneta, T. Qi, S. Chikara, S. Parkin, L. E. De Long, P. Schlottmann, and G. Cao, Electron-doped $Sr_2IrO_{4-\delta}$ ($0 \leqslant \delta \leqslant 0.04$): Evolution of a disordered $J_{\rm eff} = 1/2$ Mott insulator into an exotic metallic state, Phys. Rev. B **82**, 115117 (2010).

[52] C. Wang, H. Seinige, G. Cao, J.-S. Zhou, J. B. Goodenough, and M. Tsoi, Electrically tunable transport in the antiferromagnetic Mott insulator Sr_2IrO_4, Phys. Rev. B **92**, 115136 (2015).

[53] G. Cao, J. E. Crow, R. P. Guertin, P. F. Henning, C. C. Homes, M. Strongin, D. N. Basov, and E. Lochner, Charge density wave formation accompanying ferromagnetic ordering in quasi-one-dimensional $BaIrO_3$, Solid State Commun. **113**, 657 (2000).

[54] T. Nakano and I. Terasaki, Giant nonlinear conduction and thyristor-like negative differential resistance in $BaIrO_3$ single crystals, Phys. Rev. B **73**, 195106 (2006).